Signal transmission by vibrational resonance in one-way coupled bistable systems

Chenggui Yao[1,2] and Meng Zhan[1,*]
[1]*Wuhan Institute of Physics and Mathematics, Chinese Academy of Sciences, Whang 430071, China*
[2]*Graduate School of the Chinese Academy of Sciences, Beijing 100049, China*
(Received 8 February 2010; revised manuscript received 27 May 2010; published 21 June 2010)

Low-frequency signal transmission in one-way coupled bistable systems subject to a high-frequency force is studied. Two cases including the high-frequency force on all sites (case 1) and only on the first site (case 2) are considered. In these two cases, vibrational resonance induced by the high-frequency force can play an active role to effectively improve the signal transmission, and undamped signal transmission can be found in a broad parameter region. The combinative action of injected low-frequency signal, high-frequency driving, and coupling is of importance. Our findings suggest that high-frequency signal could be properly used in low-frequency signal transmission, and especially the implementation of high-frequency force simply on the first site for case 2 is meaningful for its simplicity and high efficiency.

DOI: 10.1103/PhysRevE.81.061129 PACS number(s): 05.40.Ca, 87.16.dj

I. INTRODUCTION

Recently, one of the great progresses in the study of nonlinear science is the finding of stochastic resonance [1–6], which reveals that noise effect is not always nuisance and noise can play a rather positive role. For example, an optimal quantity of noise can improve signal detection by a nonlinear system. Although the phenomenon with the maximal signal output at optimal strength of noise has been termed stochastic resonance, it is fundamentally different with the usual concept of (frequency) resonance in physics, which describes the tendency of a system to oscillate with larger amplitude at some resonant frequencies than at others. Due to its simplicity and robustness, stochastic resonance has attracted interdisciplinary interest and has been extensively found in a variety of systems [7–11]. In spatially extended systems, the remarkable impact of noise on signal transmission has also been investigated, such as noise enhanced propagation [12], noise sustained propagation [13], noise supported traveling wave in subexcitable media [14], and noise-induced propagation in monostable media [15]. In particular, Lindner *et al.* used noise to extend signal propagation in one- and two-dimensional arrays of two-way coupled bistable oscillators and demonstrated that moderate noise significantly extends the propagation of the periodic signal input [12]. Löcher *et al.* established the constructive role of noise on the signal transmission properties of spatially extended metastable media by studying an experimental system comprised of coupled nonlinear resonators [13]. Moreover, Zhang *et al.* [16] studied noise effect on signal transmission in one-way coupled bistable systems and found that at optimal noise intensity undamped signal transmission is possible due to the appearance of stochastic resonance. Except for these, the similar problems have already been studied by many other research groups. See, e.g., Refs. [17–19].

Analogous to noise in stochastic resonance, high-frequency signal can play a similar role [20–23]. With an optimal intensity of high-frequency signal, the system's response to a weak low-frequency signal can also become maximal. This phenomenon, called vibrational resonance, was first reported by Landa and McClintock in 2000 [20]. Since then, vibrational resonance has been intensively studied in excitable [24–27], bistable [28–31], and spatially extended systems as well [32,33]. Importantly, Chizhevsky *et al.* provided the first experimental evidence of vibrational resonance in a bistable vertical cavity laser system [34]. It is noteworthy that biharmonic signal in the context of the vibrational resonance has already been used in nature and many engineering fields. For instance, the significance of two frequency bands in long-distance vocal communication in the green treefrog (*Hyla cinerea*) was discovered several decades ago [35]. A simple two-frequency laser consisting of a laser, a half-wave plate, and an electro-optic modulator was constructed and shows high stability, easier operation, and high efficiency [36]. The nonlinear response of a gas bubble to an acoustic field consisting of a high-frequency imaging wave and an audio pumping wave was investigated by Maksimov [37]. The two-frequency coherence effect for high-frequency narrow-band pulse propagation in the fluctuating ionosphere was numerically studied [38]. Moreover, biharmonic signal transmission has been a standard technique even in the positioning and navigation in the global positioning system [39].

Although vibrational resonance resembles the usual stochastic resonance, there are some essential differences between them. The noise effect in stochastic resonance is usually described by a stochastic differential equation and characterized by stochastic process in mathematics, whereas the high-frequency signal effect in vibrational resonance is deterministic. According to a recent theoretical study [21,22], the peak in vibrational resonance is contributed by a high-frequency-signal-induced phase transition for the system switching from bistable to monostable. In contrast, stochastic resonance has long been believed to be contributed by the match of two time scales: the periodic injected signal and the Kramers rate [6]. This assumption is widely accepted, but it is in contradiction with many known numerical results and stochastic resonance in monostable systems as well. Recently, a rigorous theory of stochastic resonance was developed by Landa *et al.* [40,41], based on the fact that

*Corresponding author; zhanmeng@wipm.ac.cn

small noise in stochastic resonance or high-frequency vibration in vibrational resonance may essentially change effective system parameters with respect to slow motions. As a result, both the stochastic and vibrational resonances can be considered in a unique framework. On the other hand, vibrational resonance by a biharmonic force with very different frequencies is different with the usual frequency resonance for the coincidence of the frequency of external force with one of the natural frequencies of the system. The finding of vibrational resonance demonstrates that an unusual resonance phenomenon is still possible even if these two frequencies are sufficiently distinct.

In this work, motivated by the above-mentioned extensive engineering applications of biharmonic signal transmission and its theoretical value, we will study signal transmission in a nonlinear medium represented by one-way coupled bistable systems subject to a high-frequency signal. Similar work subject to uncorrelated noise was performed by Zhang *et al.* [16]. We are interested in the problem how the high-frequency signal influences the signal transmission, namely, how the down string sites of the one-way coupled systems respond to an excitation applied at an upper string site when a low-frequency signal is injected into the first site of the systems. Two different cases including the high-frequency force on all sites (case 1), similar to the work of Zhang *et al.*, and only on the first site (case 2) will be treated. In these two cases, the high-frequency signal indeed contributes to signal transmission greatly and undamped signal transmission can be observed broadly, while the signal damps monotonically with spatial distance without high-frequency signal. The similarity and difference between cases 1 and 2 will be compared and analyzed.

The paper is organized as follows. In Secs. II and III, we will give numerical results for case 1 and case 2, respectively. Section IV is devoted to theoretical analyses for these phenomena. Finally, a conclusion is presented in Sec. V.

II. CASE 1

First let us consider one-way coupled bistable systems with the first site driven by a low-frequency signal and each site forced by an identical high-frequency signal,

$$\dot{x}_1 = x_1 - x_1^3 + A\cos(\omega t) + B\cos(\Omega t + \phi_1), \tag{1a}$$

$$\dot{x}_i = x_i - x_i^3 + \epsilon x_{i-1} + B\cos(\Omega t + \phi_i), \quad i = 2,3,\ldots,N, \tag{1b}$$

where $A\cos(\omega t)$ indicates a low-frequency signal with amplitude A $(A \ll 1)$ and $B\cos(\Omega t+\phi_i)$ indicates a high-frequency signal of amplitude B, $\Omega \gg \omega$, and the one-way coupling strength is represented by ϵ. $\phi_i \in (-\pi, \pi)$. Without losing generality, we first consider $\phi_i=0$ for all i's. The parameter set $A=0.025$, $\omega=0.1$, $\Omega=5.0$, and $N=100$ is chosen and fixed, and the parameters B and ϵ are free. In the numerical simulations, the standard fourth-order Runge-Kutta integration algorithm with the fixed time step $\Delta t=0.01$ is used.

It is well known that the bistable media can support front propagation and it is of great significance for many processes in realistic systems [42], such as the propagation of an action potential along the axon of a nerve or the propagation of a grass fire on a prairie. Recently, front propagation under periodic forcing in reaction-diffusion systems has been studied [43,44]. Different with all of these studies, in the present work we are interested in how the additional high-frequency Ω signal influences the transmission of the low-frequency ω signal.

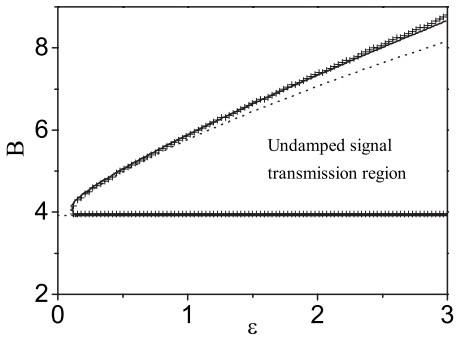

FIG. 1. Case 1 for high-frequency signal on all sites. The phase diagram for the undamped signal transmission region is surrounded by two critical (solid) curves B_{c_1} and $B_{c_2}(\epsilon)$. The curves are determined by the calculation of the gain factor in Eq. (2) relying on the information measure. The calculation and comparison based on the spectral measure give the nearly same results, as shown by the plus signs in the figure. The two dashed lines for $B_{c_1}=3.92$ and $B_{c_2}(\epsilon)$ [Eq. (15)] come from analyses. The parameters are $A=0.025$, $\omega=0.1$, $\Omega=5.0$, $N=100$, and $\phi_i=0$ $(i \geq 1)$.

A quantity Q_i chosen for describing the signal transmission in the bistable medium is defined by

$$Q_i = \sqrt{Q_{s_i}^2 + Q_{c_i}^2}/A,$$

$$Q_{s_i} = \frac{2}{nT}\int_{T_0}^{T_0+nT} x_i \sin(\omega t)dt,$$

$$Q_{c_i} = \frac{2}{nT}\int_{T_0}^{T_0+nT} x_i \cos(\omega t)dt, \tag{2}$$

where $T=\frac{2\pi}{\omega}$. A sufficiently large T_0 is chosen to discard transient processing, and $n=200$ is selected. Clearly Q_i characterizes the signal output of element i at low frequency ω. Other similar definitions of the response (including the spectral measurement) do not change the results.

As one of main results, Fig. 1 shows the phase diagram on the (ϵ, B) plane for the undamped signal transmission region, which is determined by $Q_{100} > Q_1$. From this figure, we can see that the region is well surrounded by two critical curves B_{c_1} and $B_{c_2}(\epsilon)$, and B_{c_1} $[B_{c_2}(\epsilon)]$ is independent [dependent] of ϵ. $B_{c_1} \approx 3.92$ for our parameter setting, and undamped signal transmission exists only if $B > B_{c_1}$. We also find that, as ϵ increases from zero over a critical value ϵ_c, the undamped signal transmission appears first at the optimal B $[B_{c_1} < B < B_{c_2}(\epsilon)]$, and then the B range becomes larger by further increasing ϵ. These features are very similar to those of noise effect on signal transmission [16], with B substituted

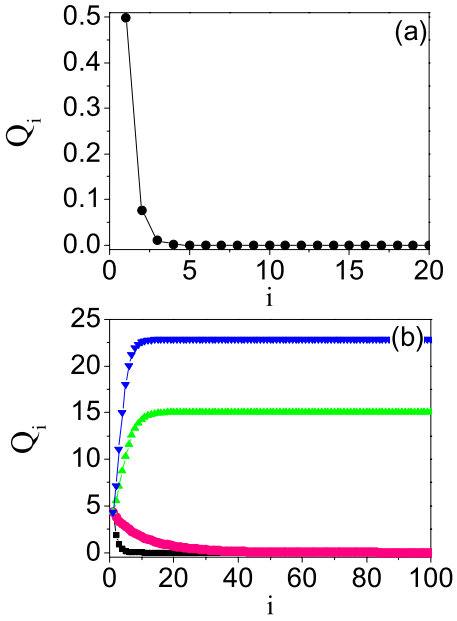

FIG. 2. (Color online) (a) and (b) Q_i vs i for the parameters (B=0, ϵ=0.4) and (B=4.5, from bottom to top, ϵ=0.1, 0.2, 0.3, and 0.4), respectively.

by the noise intensity D. The peak height of power spectrum at frequency ω for each site, P_i, was also calculated. The critical curves may also be determined by $P_{100}=P_1$ with the result depicted by plus signs in the figure. From these results, we cannot see any significant difference. Note that the relation between spectral and information measures is contradictory in some situations especially in the regime of nonlinear response [45–47]. Therefore, below we will always use the gain factor in Eq. (2) to characterize the efficiency of the signal transmission.

Figures 2(a) and 2(b) illustrate the values of Q_i for each site without high-frequency signal (B=0, ϵ=0.4) and with high-frequency signal (B=4.5, and from bottom to top ϵ =0.1, 0.2, 0.3, and 0.4), respectively. For B=0, the signal transmission is local and it damps monotonically with respect to space distance from the first site. For $B \geq B_{c_1}$, however, the signal transmission can be global and undamped if ϵ is larger than a certain threshold.

In Fig. 3, we show Q_i versus B for i=1, 2, 3, and 100; ϵ=0.4. For the first site, the usual vibrational resonance is obvious. For the down string sites, the resonance peaks become sharper and the values of Q_i increase and quickly saturate (comparing these four curves). As a result, undamped signal transmission occurs within a window for optimal value of B and it is clearly connected with the propagation of vibrational resonance.

To proceed further, we plot the time series of x_1, x_2, x_3, and x_{100} in Figs. 4(a)–4(d), respectively. A parameter set (B =4.5, ϵ=1.5) is arbitrarily chosen within the undamped signal transmission region. In all these figures, the low-frequency periodic signal with the period T ($T=\frac{2\pi}{\omega}\approx 62.8$) is modulated by a high-frequency signal with the period T' ($T'=\frac{2\pi}{\Omega}\approx 1.3$). The amplitude of the high-frequency signal is constant. However, that of the low-frequency signal increases rapidly with the increase in i; this finding accords with the observations in Figs. 2(b) and 3. Therefore, we know that in certain conditions the high-frequency force contributes to signal transmission and plays a similar constructive role as noise.

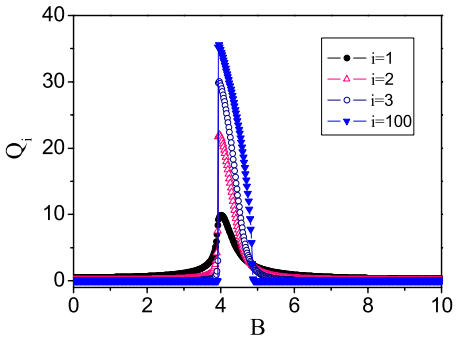

FIG. 3. (Color online) Q_i vs B for i=1, 2, 3, and 100; ϵ=0.4. Vibrational resonance enhanced signal propagation is clear at optimal value of B.

Finally, the effect of additional initial phases ϕ_i's in Eqs. (1a) and (1b) is studied. Clearly the addition of ϕ_1 in Eq. (1a) does not change the dynamics of x_1 as A is small compared to B. However, the addition of ϕ_i in Eq. (1b) does change the dynamics of x_i ($i \geq 2$) due to the input of the ϵx_{i-1} term in the equation. In Figs. 5(a)–5(c), we show the phase diagrams for the undamped signal transmission region, after we consider three different sets of random values of ϕ_i ($-\pi \leq \phi_i \leq \pi$). The critical (solid) curves, same as in Fig. 1 for ϕ_i=0, are also superimposed. They are different, especially for larger values of ϵ, indicating that the effect of additional initial phases is significant. Next the effect of the rational or irrational ratio Ω/ω is studied. The results are shown in Fig. 5(d), where—from bottom to top—the critical curves are for three different values of Ω: $\Omega=2\sqrt{2}$, 4, and 5, respectively. ω=0.1 is fixed; ϕ_i=0 ($i \geq 1$). They can be viewed as translated in the ordinate; this point can be well predicated by our following theories. From these plots, we cannot see any significant change for irrational ratios except for a scale change.

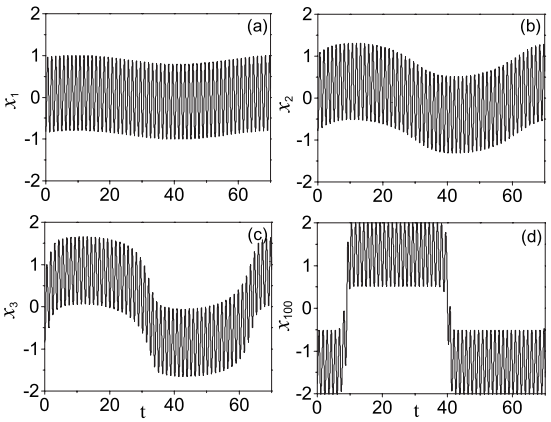

FIG. 4. (a)–(d) The time series of x_1, x_2, x_3, and x_{100}, respectively, showing an increasing low-frequency signal amplitude, with a constant amplitude modulation of high-frequency signal. B=4.5 and ϵ=1.5 within the undamped signal transmission region.

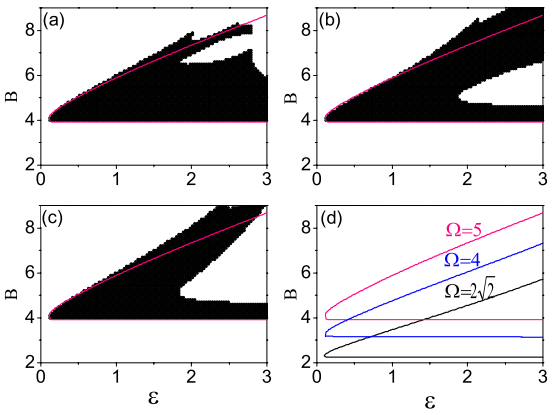

FIG. 5. (Color online) (a)–(c) The phase diagrams (black points) for the undamped signal transmission region, considering the effect of additional initial phases ϕ_i's in Eq. (1b). For different random values of ϕ_i ($-\pi \leq \phi_i \leq \pi$), they are different with each other and all of them are different with the phase diagram (solid lines) for $\phi_i=0$ as in Fig. 1. (d) The critical curves for $\Omega=2\sqrt{2}$, 4, and 5 (from bottom to top). $\omega=0.1$ is fixed; $\phi_i=0$ ($i \geq 1$).

III. CASE 2

In this section, we will study the same problem as in Sec. II, but with only the first element driven by a high-frequency force. The equations become

$$\dot{x}_1 = x_1 - x_1^3 + A\cos(\omega t) + B\cos(\Omega t + \phi_1), \tag{3a}$$

$$\dot{x}_i = x_i - x_i^3 + \epsilon x_{i-1}, \quad i = 2,3,\ldots,N. \tag{3b}$$

Obviously different values of ϕ_1 do not change the dynamics of x_1 as A is small compared to B; below we will set $\phi_1=0$ for simplicity. Figure 6 shows the undamped signal transmission region, which is surrounded by several critical (heavy solid) lines. The two critical (thin) lines for case 1 are also superimposed. One may intuitively believe that case 2 with only the first element driven by a high-frequency force should have a weaker effect on signal transmission, compared to case 1 with all elements driven by a high-frequency force, or even cannot support signal transmission. The pattern in Fig. 6, however, gives a completely opposite result.

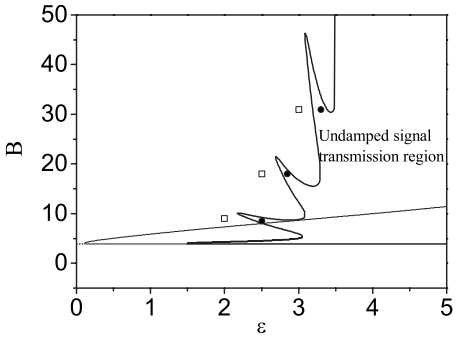

FIG. 6. Phase diagram for case 2 with high-frequency signal on the first site only. The maplelike shape of critical curves (heavy solid lines) is clear. In contrast, the two critical curves (thin lines) for case 1 at small B are superimposed.

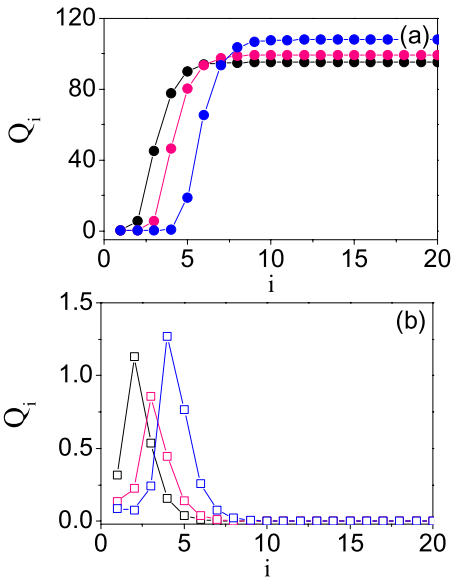

FIG. 7. (Color online) (a) and (b) Q_i vs i for the parameters within and out of the undamped signal transmission region, respectively. In (a), from left to right, the three curves correspond to (B=9.0, ϵ=2.5), (B=18.0, ϵ=2.8), and (B=31.0, ϵ=3.4), In (b), from left to right, (B=9.0, ϵ=2.0), (B=18.0, ϵ=2.5), and (B=31.0, ϵ=3.0). These parameters are denoted by filled circles and open squares in Fig. 6, respectively.

Instead, case 2 shows a much larger undamped signal transmission region. The region expands tremendously to larger values of B, with the same unchanged lower threshold B_{c_1} ($B_{c_1} \approx 3.92$) and a larger ϵ_c. Meanwhile, the edge of region becomes complicated, showing a maplelike shape. It is notable that if only the first element is driven by noise, no undamped signal transmission exists for any D and ϵ.

Figures 7(a) and 7(b) plot Q_i versus i for the parameters within the undamped signal transmission region [from left to right: (B=9, ϵ=2.5), (B=18, ϵ=2.8), and (B=31, ϵ=3.4), as shown by the three circles in Fig. 6] and out of the region [from left to right: (B=9, ϵ=2.0), (B=18, ϵ=2.5), and (B=31, ϵ=3.0), as shown by the three squares in Fig. 6], respectively. Different with the monotonic increase or decrease in Q_i, in Fig. 2(b) for case 1, a slight increase for the first several sites is discernible from both Figs. 7(a) and 7(b). Note that these two panels have very different scales in their ordinates.

Further, we plot Q_i vs B for ϵ=1.0, 2.0, 2.5, and 4.0 in Figs. 8(a)–8(d), respectively. In Fig. 8(a), Q_{100} vanishes as ϵ is smaller than the threshold. In contrast, the patterns of vibrational resonance with a monopeak [Fig. 8(b)], bipeak [Fig. 8(c)], and plateau [Fig. 8(d)] for $B > B_{c1}$ are clear. In the inset of Fig. 8(b), the part of the damp of the second resonance peak is enlarged. In Figs. 8(c) and 8(d), the regions of undamped signal transmission become much larger. All of them look quite different with those for case 1 in Fig. 3.

Finally, the time series of x_i for ϵ=2.0 and 4.0 are displayed in Figs. 9(a) and 9(b), respectively. B=5.0 is the same. In Fig. 9(a), from bottom to top, the five curves correspond to i=2, 3, 4, 5, and 100. Different with the vanishing

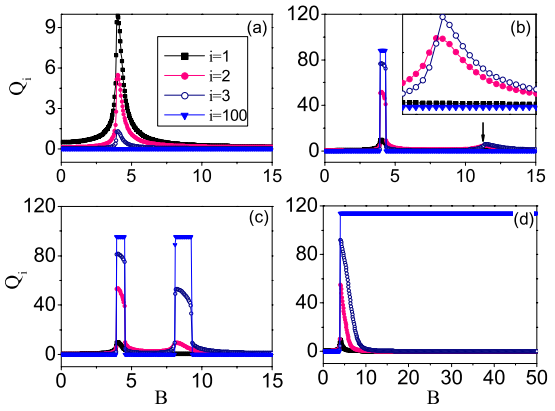

FIG. 8. (Color online) (a)–(d) The plots of Q_i vs B for ϵ=1.0, 2.0, 2.5, and 4.0, respectively. The vibrational resonance propagation shows some new features with that for case 1 in Fig. 3. The inset of (b) shows the zoomed-in part of the damp of the second resonance peak.

of low-frequency signal in Fig. 9(a), in Fig. 9(b) the propagation of low-frequency signal has been established and become undamped. We also find that now the high-frequency signal fades with the propagation, which is essentially different with that in case 1 [comparing x_{100} in Fig. 9(b) and that in Fig. 4(d)].

In Ref. [24], Ullner *et al.* reported vibrational resonance and vibrational propagation in excitable systems by studying an excitable electronic circuit and the FitzHugh-Nagumo model. In their studies, every oscillator in the chain is driven by an identical high-frequency signal, which corresponds to case 1 (not case 2) in our model study. The phenomena for the signal propagation are quite similar. Except for the different systems, some other distinctions are clear. For instance, their report on resonant vibrational propagation is brief with only a single example, whereas our studies will rely on not only numerical observations but also theoretical analyses.

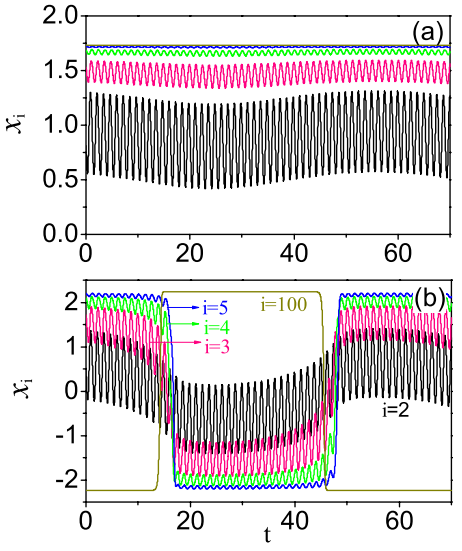

FIG. 9. (Color online) (a) and (b) The time series of x_i for the parameters (ϵ=2.0, B=5.0) within and (ϵ=4.0, B=5.0) out of the undamped signal transmission region. In (a), from bottom to top, i=2, 3, 4, 5, and 100. In (b), with the increase in i, the amplitude of low-frequency signal increases and that of high-frequency signal decreases.

All the differences between cases 1 and 2 need an explanation and the underlying mechanisms of undamped signal transmission for these two cases should be elucidated clearly by theoretical analyses. This is exactly the objective of our next section.

IV. THEORETICAL ANALYSES

The vibrational resonance in single bistable systems has been well analyzed in [21,22], based on the method of inertial approximation [23]. The basic idea behind this method is that the system variable under the condition of high-frequency signal force can be decomposed into a slow motion and a fast motion. Thus, in the bistable systems, the high-frequency signal changes the dynamics of the slow motion and gives rise to a system transition from bistable to monostable, which further makes the amplitude of the slow component (signal) of the output of the systems at the transition point become maximal.

In this work, we generalize this method for the study of signal transmission in one-way coupled bistable systems. Since the effect of additional initial phase ϕ_i's in Eq. (1b) for case 1 is very complicated, as shown in Figs. 5(a)–5(c), in the following analyses we will only consider ϕ_i=0 ($i \geq 1$). For the first site, $x_1(t)$ in Eq. (1a) [or in Eq. (3a)] can be decomposed into a slow motion $X_1(t)$ with frequency ω and a fast motion $\Psi_1(t)$ with frequency Ω,

$$x_1(t) = X_1(t) + \Psi_1(t). \tag{4}$$

Substituting this equation into Eq. (1a), we obtain the following evolution equations for $X_1(t)$ and $\Psi_1(t)$:

$$\dot{X}_1 - X_1 + X_1^3 + 3X_1\overline{\Psi_1^2} + \overline{\Psi_1^3} = A\cos(\omega t), \tag{5a}$$

$$\dot{\Psi}_1 - \Psi_1 + 3X_1^2\Psi_1 + 3X_1(\Psi_1^2 - \overline{\Psi_1^2}) + \Psi_1^3 - \overline{\Psi_1^3} = B\cos(\Omega t), \tag{5b}$$

where the overbar denotes time integral within a period T' ($T' = 2\pi/\Omega$).

Remembering that Ψ_1 is a rapidly changing force, we have

$$\dot{\Psi}_1 \gg \Psi_1, \Psi_1^2, \Psi_1^3, \tag{6}$$

which leads to

$$\dot{\Psi}_1 = B\cos(\Omega t), \tag{7}$$

and further

$$\Psi_1 = \frac{B}{\Omega}\sin(\Omega t). \tag{8}$$

Taking into account that $\overline{\Psi_1^3}$=0 and $\overline{\Psi_1^2}$=$B^2/2\Omega^2$, Eq. (5a) becomes

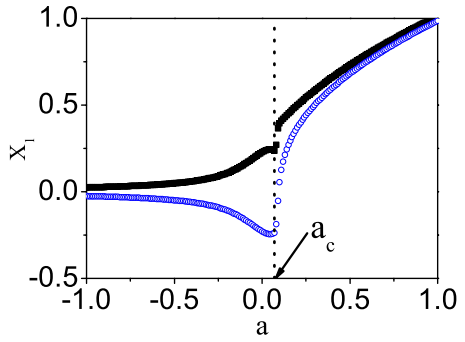

FIG. 10. (Color online) Bifurcation diagram of $X_1(t)$ [Eq. (10)] for the maximal (square points) and minimal (circular points) values. $A=0.025$ and $\omega=0.1$. In the presence of A ($A \ll 1$ but $A \neq 0$), a critical a_c ($a_c \approx 0.078 \neq 0$) exists, indicative of a transition of system behavior from monostable to bistable, and also from symmetric to asymmetric. From this figure, we obtain a more precise estimation: $B_{c_1} \approx 3.92$.

$$\dot{X}_1 = \left(1 - \frac{3B^2}{2\Omega^2}\right) X_1 - X_1^3 + A\cos(\omega t). \tag{9}$$

Clearly the high-frequency signal intensity B has come into the linear term of the equation and will change the low-frequency signal output. For convenience, Eq. (9) can be rewritten in the following form:

$$\dot{X}_1 = aX_1 - X_1^3 + A\cos(\omega t), \tag{10}$$

where

$$a = 1 - \frac{3B^2}{2\Omega^2}. \tag{11}$$

Under the condition $A=0$, the system of X_1 is bistable with two symmetric equilibria ($X_1 = \pm\sqrt{a}$) if $a>0$, or it is monostable with only one equilibrium at the origin ($X_1=0$) if $a<0$. Immediately, we may have prediction of a transition point $a_c=0$ and, equivalently, $B_c = \Omega\sqrt{2(1-a_c)/3} = \Omega\sqrt{\frac{2}{3}}$. As $\Omega=5.0$, $B_c = 4.08 > B_{c_1} \approx 3.92$.

For a small but nonzero A, X_1 will show a periodic oscillation with small amplitude and frequency ω around one equilibrium ($X_1=\sqrt{a}$ or $X_1=-\sqrt{a}$) if the system is bistable, or around the origin ($X_1=0$) if the system is monostable. In Fig. 10, we plot the bifurcation diagram of the maximal and minimal values of $X_1(t)$ [Eq. (10)] with the change in a. $A=0.025$ and $\omega=0.1$. A critical a_c exists, indicative of a transition of system behavior from monostable to bistable, and also from symmetric to asymmetric. Here, $a_c = 0.078 \neq 0$, due to the influence of a small A. Based on this observation, now we have a more precise estimation: $B_c = \Omega\sqrt{2(1-a_c)/3} = 3.92$, which is equal to B_{c_1}. Therefore, we know that the monostablitity (or symmetricity) of the first site X_1 is one of the necessary conditions for the undamped signal transmission down the string, and the bistability (or asymmetricity) of X_1 can only spoil the signal transmission. This is right; the phase diagrams for both cases 1 and 2 in Fig. 6 prove this point well.

Furthermore, eliminating the third-order term in Eq. (10) and solving X_1, we explicitly have

$$X_1(t) = \frac{A\cos(\omega t - \theta_1)}{\sqrt{\omega^2 + a^2}}, \tag{12}$$

with $\theta_1 = \arctan\frac{\omega}{a}$, under the conditions $B > B_{c_1}$ and $A \ll 1$. For case 1, we may further apply the approximation method for variable decomposition $[x_1(t) = X_1(t) + \Psi_1(t)]$ to all down sites and obtain

$$\dot{X}_i = aX_i - X_i^3 + \epsilon X_{i-1}, \tag{13a}$$

$$\Psi_i = \frac{B}{\Omega}\sin(\Omega t), \quad i = 2, \ldots, N, \tag{13b}$$

under the condition $\epsilon \ll 1$.

Comparing Eq. (13a) for $i=2$ and Eq. (10) for $i=1$ and considering the solution of X_1 in Eq. (12), we have if

$$\frac{\epsilon A}{\sqrt{\omega^2 + a^2}} \geq A, \tag{14}$$

then $Q_2 \geq Q_1$. If this inequality is satisfied, we may even have $Q_i \geq Q_{i-1}$ for all $i \geq 2$. Therefore, from Eq. (14) the other critical curve for the undamped signal transmission in Fig. 1 should be determined by

$$B_{c_2}(\epsilon) = \Omega\sqrt{\frac{2(1 + \sqrt{\epsilon^2 - \omega^2})}{3}}. \tag{15}$$

The agreement of the dashed line from this equation with the solid line from the data is well verified in Fig. 1. Besides, the minimum $\epsilon_c = \omega = 0.1$ is clear. Now it is also quite natural to understand the monotonic increase in Q_i in Figs. 2(b) and 3, for the parameters ϵ and B chosen within the undamped signal transmission region. Moreover, from Eq. (13b), the phenomenon of undamped high-frequency signal amplitude, as shown in Fig. 4, is easy to understand.

Next let us analyze case 2. Compared to case 1, the undamped signal transmission region for case 2 becomes greatly enlarged in the B direction. Therefore, we have to reconsider the similar problem but with much larger value of B. Some approximation relations do not exist, e.g., Eq. (6). From Eq. (5b), eliminating the crossing terms (based on $B \gg A$), we have

$$\dot{\Psi}_1 = \Psi_1 - \Psi_1^3 + B\cos(\Omega t). \tag{16}$$

Supposing that the form of $\Psi_1(t)$ is

$$\Psi_1(t) = C_1\sin(\Omega t - \Theta_1), \tag{17}$$

we further obtain that the value of C_1 should be determined by

$$C_1\Omega = B\cos(\Theta_1), \tag{18a}$$

$$C_1 - C_1^3 = B\sin(\Theta_1). \tag{18b}$$

Consequently,

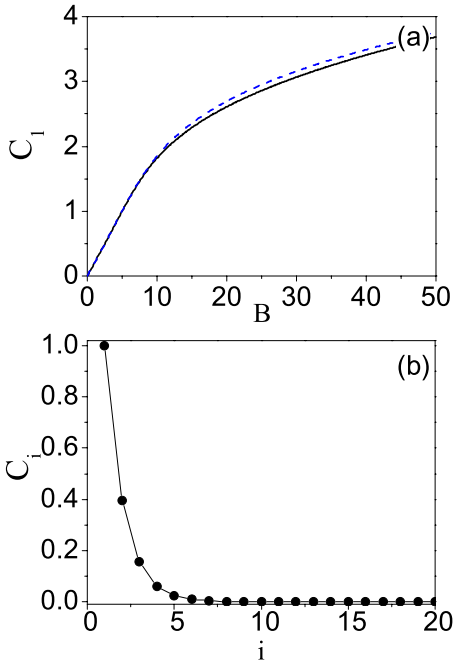

FIG. 11. (Color online) (a) C_1 vs B. The solid line from numerical calculation of the amplitude of Ψ_1 in Eq. (16) and the dashed line from theory in Eq. (20a) are compared. (b) C_i vs i, showing a monotonic decrease relation. $B=5.0$ and $\epsilon=2.0$. For more details, see the text.

$$(C_1\Omega)^2 + (C_1 - C_1^3)^2 = B^2. \tag{19}$$

Relying on the Cardano formula, we solve the above equation and get

$$C_1 = \sqrt{\frac{2}{3} + (T_1 + \sqrt{D_1})^{1/3} + (T_1 - \sqrt{D_1})^{1/3}}, \tag{20a}$$

$$T_1 = -\frac{2(\Omega^2+1)/3 - B^2 - 16/27}{2}, \tag{20b}$$

$$D_1 = T_1^2 + \left(\frac{\Omega^2 - 1/3}{3}\right)^3. \tag{20c}$$

The numerical result (solid line) for the amplitude of Ψ_1 in Eq. (16) and the theoretical (dashed) curve for C_1 vs B from the above equations are shown in Fig. 11(a). The fit is good. If B ($B<10$) is small, both curves show a linear relation between C_1 and B ($C_1 \approx \frac{B}{\Omega}$). If B becomes larger, however, a small deviation is clear.

For the slow variable X_1, further we have

$$\dot{X}_1 = \left(1 - \frac{3C_1^2}{2}\right)X_1 - X_1^3 + A\cos(\omega t). \tag{21}$$

The only difference with Eq. (9) for case 1 is that $\frac{B}{\Omega}$ in Eq. (9) is substituted by C_1 now.

For all other sites, similarly X_i and Ψ_i are controlled by

$$\dot{X}_i = \left(1 - \frac{3C_i^2}{2}\right)X_i - X_i^3 + \epsilon X_{i-1}, \tag{22a}$$

$$\Psi_i = C_i \sin(\Omega t - \Theta_i), \quad i = 2, \ldots, N, \tag{22b}$$

with

$$C_i = \sqrt{\frac{2}{3} + (T_i + \sqrt{D_i})^{1/3} + (T_i - \sqrt{D_i})^{1/3}}, \tag{23a}$$

$$T_i = -\frac{2(\Omega^2+1)/3 - (\epsilon C_{i-1})^2 - 16/27}{2}, \tag{23b}$$

$$D_i = T_i^2 + \left(\frac{\Omega^2 - 1/3}{3}\right)^3, \tag{23c}$$

and

$$C_0 = \frac{B}{\epsilon}.$$

Obviously the key difference between cases 1 and 2 is that now the evolution equations of X_i and Ψ_i for all i's are determined by the value of C_i (not $\frac{B}{\Omega}$). C_i depends on B, ϵ, and i, and it can only be numerically calculated. The result is shown in Fig. 11(b), where the monotonic decrease relation between C_i and i is clear. $B=5.0$ and $\epsilon=2.0$. Due to the complicated form of C_i, we cannot derive more analytical results as we do for case 1, but we can still obtain some qualitative results. For instance, Eq. (22b) tells us that the information of high-frequency signal will damp with the increase in i; this is exactly what we see in Fig. 9(b). As i increases, C_i decreases and $1-3C_i^2/2$ increases ($1-3C_i^2/2 < 0$ for the first several i's), which will produce a larger amplitude of X_i, as shown in Fig. 10. Therefore, it is easy to understand the monotonic increase in Q_i for the first several sites in Figs. 7(a) and 7(b). When i increases further, a transition from monostable to bistable for X_i appears and $C_i \approx 0$ for all large i's. From Eq. (22a), we can predict that a sufficiently large coupling ϵ may support undamped Q_i; the pattern that a large undamped signal transmission region exists if $\epsilon > 3.49$ and $B < 50$ in Fig. 6 proves this point well. Prior to $\epsilon \approx 3.49$, the multipeak structure with the maplelike shape reflects the complicated competition relation between B and ϵ due to the change in the value of $C_i(B,\epsilon)$ for the first several sites.

V. CONCLUSION

In conclusion, we have studied signal transmission in a nonlinear medium described by a classical model of one-way coupling bistable systems subject to a high-frequency signal. The numerical results, supplemented by the theoretical analyses, show that high-frequency signal can contribute to the transmission of low-frequency signal with the help of vibrational resonance. Compared to noise in signal transmission, the high-frequency signal input is deterministic and is more controllable. Although the study in the paper is based on a purely abstract consideration, some applications are expected. Since the technique with a low-frequency signal modulated by a high-frequency carrier signal has already been applied in acoustics, neuroscience, laser, electronic circuits, and many engineering fields [36–39], we hope that the

findings in the paper are valuable to these fields. Some realizations in optical systems and neural networks are the best candidates. In particular, the scheme with a high-frequency signal only on the first site could be of great significance for potential applications due to its simplicity and high efficiency.

ACKNOWLEDGMENTS

This work was partially supported by the Bairen Jihua Foundation of Chinese Academy of Sciences (M.Z.). We thank the anonymous referees very much for comments and suggestions.

[1] K. Wiesenfeld and F. Moss, Nature (London) **373**, 33 (1995).
[2] P. Jung and P. Hänggi, Phys. Rev. A **44**, 8032 (1991).
[3] Hu Gang, H. Haken, and C. Z. Ning, Phys. Rev. E **47**, 2321 (1993).
[4] B. McNamara, K. Wiesenfeld, and R. Roy, Phys. Rev. Lett. **60**, 2626 (1988).
[5] L. Gammaitoni, M. Locher, A. Bulsara, P. Hänggi, J. Neff, K. Wiesenfeld, W. Ditto, and M. E. Inchiosa, Phys. Rev. Lett. **82**, 4574 (1999).
[6] L. Gammaitoni, P. Hänggi, P. Jung, and F. Marchesoni, Rev. Mod. Phys. **70**, 223 (1998).
[7] A. S. Pikovsky and J. Kurths, Phys. Rev. Lett. **78**, 775 (1997).
[8] J. M. G. Vilar and J. M. Rubi, Phys. Rev. Lett. **77**, 2863 (1996).
[9] P. C. Gailey, A. Neiman, J. J. Collins, and F. Moss, Phys. Rev. Lett. **79**, 4701 (1997).
[10] Hu Gang, T. Ditzinger, C. Z. Ning, and H. Haken, Phys. Rev. Lett. **71**, 807 (1993).
[11] A. Pikovsky, A. A. Zaikin, and M. A. de la Casa, Phys. Rev. Lett. **88**, 050601 (2002).
[12] J. F. Lindner, S. Chandramouli, A. R. Bulsara, M. Löcher, and W. L. Ditto, Phys. Rev. Lett. **81**, 5048 (1998).
[13] M. Löcher, D. Cigna, and E. R. Hunt, Phys. Rev. Lett. **80**, 5212 (1998).
[14] S. Kádár, J. Wang, and K. Showalter, Nature (London) **391**, 770 (1998).
[15] A. A. Zaikin, J. García-Ojalvo, L. Schimansky-Geier, and J. Kurths, Phys. Rev. Lett. **88**, 010601 (2001).
[16] Y. Zhang, G. Hu, and L. Gammaitoni, Phys. Rev. E **58**, 2952 (1998).
[17] R. Báscones, J. García-Ojalvo, and J. M. Sancho, Phys. Rev. E **65**, 061108 (2002).
[18] J. Armero, J. M. Sancho, J. Casademunt, A. M. Lacasta, L. Ramirez-Piscina, and F. Sagués, Phys. Rev. Lett. **76**, 3045 (1996).
[19] M. Löcher, N. Chatterjee, F. Marchesoni, W. L. Ditto, and E. R. Hunt, Phys. Rev. E **61**, 4954 (2000).
[20] P. S. Landa and P. V. E. McClintock, J. Phys. A **33**, L433 (2000).
[21] J. P. Baltanás, L. López, I. I. Blechman, P. S. Landa, A. Zaikin, J. Kurths, and M. A. F. Sanjuán, Phys. Rev. E **67**, 066119 (2003).
[22] I. I. Blekhman and P. S. Landa, Int. J. Non-Linear Mech. **39**, 421 (2004).
[23] I. I. Blekhman, *Vibrational Mechanics: Nonlinear Dynamic Effects, General Approach, Applications* (World Scientific, Singapore, 2000).
[24] E. Ullner, A. Zaikin, J. García-Ojalvo, R. Bascones, and J. Kurths, Phys. Lett. A **312**, 348 (2003).
[25] C. Stan, C. P. Cristescu, D. Alexandroaei, and M. Agop, Chaos, Solitons Fractals **41**, 727 (2009).
[26] D. Cubero, J. P. Baltanás, and J. Casado-Pascual, Phys. Rev. E **73**, 061102 (2006).
[27] B. Deng, J. Wang, and X. L. Wei, Chaos **19**, 013117 (2009).
[28] J. Casado-Pascual and J. P. Baltanás, Phys. Rev. E **69**, 046108 (2004).
[29] V. N. Chizhevsky and G. Giacomelli, Phys. Rev. E **73**, 022103 (2006).
[30] V. N. Chizhevsky and G. Giacomelli, Phys. Rev. E **70**, 062101 (2004).
[31] V. N. Chizhevsky and G. Giacomelli, Phys. Rev. A **71**, 011801(R) (2005).
[32] A. A. Zaikin, L. López, J. P. Baltanás, J. Kurths, and M. A. F. Sanjuán, Phys. Rev. E **66**, 011106 (2002).
[33] V. M. Gandhimathi, S. Rajasekar, and J. Kurths, Phys. Lett. A **360**, 279 (2006).
[34] V. N. Chizhevsky, E. Smeu, and G. Giacomelli, Phys. Rev. Lett. **91**, 220602 (2003).
[35] H. C. Gerhardt, Nature (London) **261**, 692 (1976).
[36] D. Su, M. Chiu, and C. Chen, Precis. Eng. **18**, 161 (1996).
[37] A. Maksimov, Ultrasonics **35**, 79 (1997).
[38] V. Gherm, N. Zernov, B. Lundborg, and A. Vastberg, J. Atmos. Sol.-Terr. Phys. **59**, 1831 (1997).
[39] E. D. Kaplan, *Understanding GPS: Principles and Applications* (Artech House, London, 1996).
[40] P. S. Landa, V. Ushakova, and J. Kurths, Chaos, Solitons Fractals **30**, 574 (2006).
[41] P. S. Landa, I. A. Khovanov, and P. V. E. McClintock, Phys. Rev. E **77**, 011111 (2008).
[42] J. Keener and J. Sneyd, *Mathematical Physiology* (Springer, Berlin, 1998), Chap. 9.
[43] F. G. Bass and R. Bakanas, EPL **53**, 444 (2001).
[44] E. P. Zemskov, K. Kassner, and S. C. Müller, Eur. Phys. J. B **34**, 285 (2003).
[45] M. I. Dykman, R. Mannella, P. V. E. McClintock, N. D. Stein, and N. G. Stocks, Phys. Rev. E **47**, 1629 (1993).
[46] I. A. Khovanov and P. V. E. McClintock, Phys. Rev. E **76**, 031122 (2007).
[47] I. A. Khovanov, Phys. Rev. E **77**, 011124 (2008).